# Journal Pre-proof


Design, synthesis and biological evaluation of novel potent STAT3 inhibitors based on BBI608 for cancer therapy

Kai-Rui Feng, Feng Wang, Xin-Wei Shi, Yun-Xuan Tan, Jia-Ying Zhao, Jian-Wei Zhang, Qing-Hua Li, Guo-Qiang Lin, Dingding Gao, Ping Tian

PII: S0223-5234(20)30399-8

DOI: https://doi.org/10.1016/j.ejmech.2020.112428

Reference: EJMECH 112428

To appear in: *European Journal of Medicinal Chemistry*

Received Date: 17 January 2020

Revised Date: 24 April 2020

Accepted Date: 5 May 2020

Please cite this article as: K.-R. Feng, F. Wang, X.-W. Shi, Y.-X. Tan, J.-Y. Zhao, J.-W. Zhang, Q.-H. Li, G.-Q. Lin, D. Gao, P. Tian, Design, synthesis and biological evaluation of novel potent STAT3 inhibitors based on BBI608 for cancer therapy, *European Journal of Medicinal Chemistry* (2020), doi: https://doi.org/10.1016/j.ejmech.2020.112428.

# Design, synthesis and biological evaluation of novel potent STAT3 inhibitors based on BBI608 for cancer therapy

Kai-Rui Feng [#], Feng Wang [#], Xin-Wei Shi, Yun-Xuan Tan, Jia-Ying Zhao, Jian-Wei Zhang, Qing-Hua Li *, Guo-Qiang Lin, Dingding Gao *, and Ping Tian *

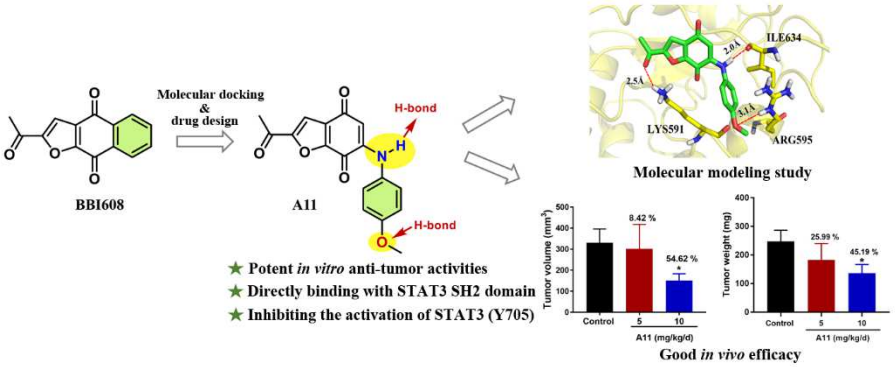

# Design, synthesis and biological evaluation of novel potent STAT3 inhibitors based on BBI608 for cancer therapy

Kai-Rui Feng [a, #], Feng Wang [a, #], Xin-Wei Shi [a], Yun-Xuan Tan, [b] Jia-Ying Zhao [a], Jian-Wei Zhang [a], Qing-Hua Li [a, *], Guo-Qiang Lin [a, b], Dingding Gao [a, *], and Ping Tian [a, b, *]

[a] *The Research Center of Chiral Drugs, Innovation Research Institute of Traditional Chinese Medicine, Shanghai University of Traditional Chinese Medicine, Shanghai 201203, China*

[b] *CAS Key Laboratory of Synthetic Chemistry of Natural Substances, Center for Excellence in Molecular Synthesis, Shanghai Institute of Organic Chemistry, University of Chinese Academy of Sciences, Chinese Academy of Sciences, Shanghai 200032, China*

[#] These authors contributed equally to this work.

* Corresponding authors:

*E-mail* addresses: gaodingding@shutcm.edu.cn (Dingding Gao), qinghuali@shutcm.edu.cn (Qing-Hua Li), tianping@shutcm.edu.cn (Ping Tian)

**Abstract:** Persistently activated signal transducer and activator of transcription 3 (STAT3) plays an important role in the development of multiple cancers, and therefore is a potential therapeutic target for cancer prevention. Herein, we report the rational design, synthesis, and biological evaluation of novel potent STAT3 inhibitors based on BBI608. Among them, compound **A11** exhibited the most potent *in vitro* tumor cell growth inhibitory activities toward MDA-MB-231, MDA-MB-468 and HepG2 cells with $IC_{50}$ values as low as 0.67±0.02 μM, 0.77±0.01 μM and 1.24±0.16 μM, respectively. Fluorescence polarization (FP) assay validated the binding of compound **A11** in STAT3 SH2 domain with the $IC_{50}$ value of 5.18 μM. Further mechanistic studies indicated that **A11** inhibited the activation of STAT3 (Y705), and thus reduced the expression of STAT3 downstream genes CyclinD1 and C-Myc. Simultaneously, it induced cancer cell S phase arrest and apoptosis in a concentration-dependent manner. An additional *in vivo* study revealed that **A11** suppressed the MDA-MB-231 xenograft tumor growth in mice at the dose of 10 mg/kg (i.p.) without obvious body-weight loss. Finally, molecular docking study further elucidated the binding mode of **A11** in STAT3 SH2 domain.

**Keywords**: STAT3 inhibitors; BBI608; anti-tumor activity; molecular docking.

## 1. Introduction

Signal transducer and activator of transcription 3 (STAT3) is a member of the STAT family and play a pivotal role in tumor initiation, progression and maintenance [1-4]. Once upon activated by upstream kinases (growth factor receptors, tyrosine kinases, Janus kinases, Src family kinases, etc.), STAT3 monomers are phosphorylated at specific tyrosine residues (Y705) in the C-terminal domain and form transcriptionally active homodimers in a symmetric reciprocal manner. Then these homodimers translocate into the nucleus and bind to a specific DNA sequence, regulating target genes transcription [5-7,]. Abnormally activated STAT3 signaling is found in a variety of solid tumors and hematological malignancies, and can induce tumor angiogenesis and suppresses anti-tumor immune responses [8-11]. In addition, aberrant STAT3 correlates with resistance to chemotherapy and poor prognosis [12,13]. Abundant evidence suggests that STAT3 is an ideal target for cancer therapy, and various small inhibitors were identified using multiple approaches [14], such as STA-21 [15], LLL-12 [16], LY-5 [17], Stattic [18], Niclosamide [19], S3I-201 [20], S3I-201-1066 [21], **8** [22], BBI608 [23], and other representative STAT3 inhibitors [24-31]. It is worth noting that Wang and co-workers have recently reported some potent, selective, and efficacious small-molecule STAT3 degraders based upon the proteolysis targeting chimera (PROTAC) concept [32,33]. However, there has been no STAT3-targeting drug approved by the FDA to date. This may be partly due to the lack of understanding of signaling crosstalk and adverse events related to STAT3-specific activity in normal tissues. Also, the scarcity of membrane permeability and stability, and weak binding affinity were found to be the main roadblocks of these inhibitors [34-36]. Consequently, development of novel potent STAT3 inhibitors will bring enormous challenges and opportunities in the cancer prevention field.

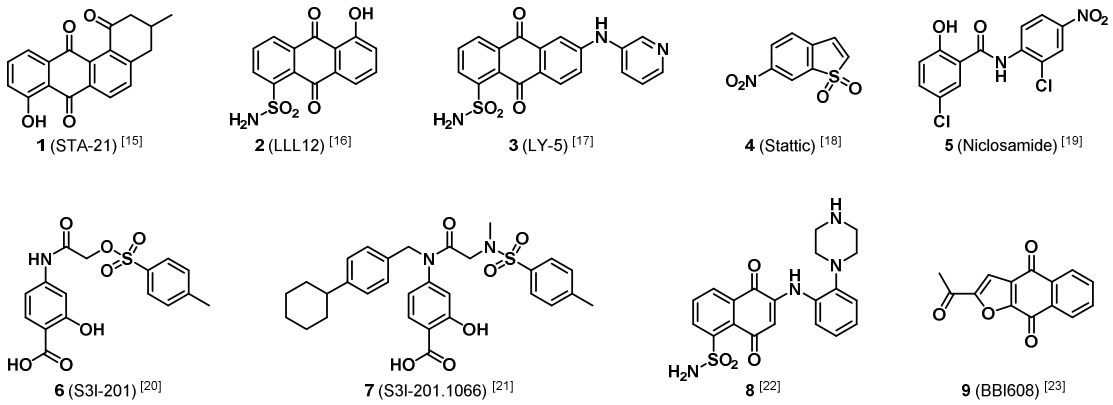


**Fig. 1.** Representative of known STAT3 inhibitors

Among all the reported STAT3 inhibitors, only BBI608 (Napabucasin) has been shown to block cancer stem cell pathway activity and is currently in Phase II/III clinical trials for the treatment of a variety of cancers [37]. To our knowledge, the previous structural modifications of BBI608 mainly focused on the acetyl group at 2-position of furan ring [38-42] (Fig. 2), and lack of structural diversity. These finding prompted us to develop new BBI608 derivatives with novel scaffolds and potent antitumor activities using structure-based drug design in this work. Firstly, BBI608 was docked into STAT3 SH2 domain (PDB code: 1BG1) and the binding mode was shown in Fig. 3A. The 2-acetylfuran group was located at the pY705 (also named pY+0) site, which is related to the disruption of STAT3 phosphorylation and dimerization of inhibitors, and formed a hydrogen bond with Arg609. However, the other important pocket (pY+X site) stayed vacant and was not occupied by any other group. Accordingly, to improve the binding affinity and find new STAT3 inhibitors, the benzene ring in BBI608 was selected to be cleaved and diverse functional groups were directly introduced into the quinone ring via suitable linkers for reaching the pY+X site (Fig. 2). The binding modes of designed compounds harboring different linkers (**a1**–**a5**) were predicted using docking studies and shown in Fig. 3B–3F. Considering that the free amine, ie -NH- (linker **a1**), in the compound **A1** could form hydrogen bond with ILE634, **a1** was determined as a privileged linker. As a consequence, various benzene ring derivatives and fragments were then carefully investigated.

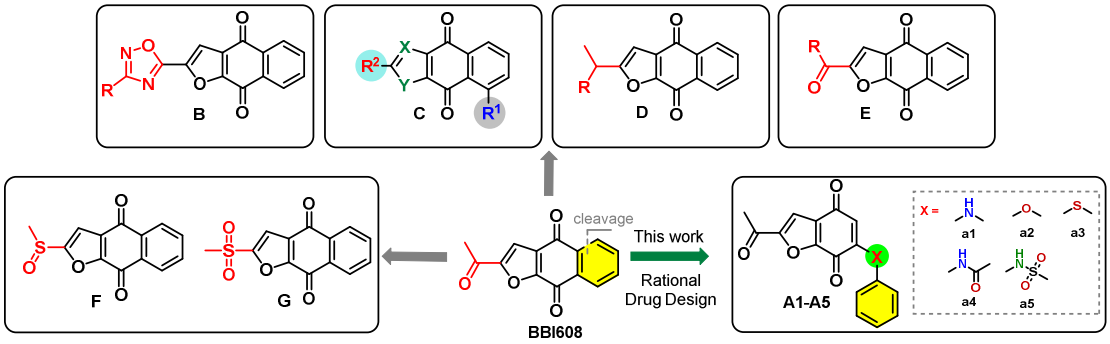


**Fig. 2.** Previous and our structure-based drug design of STAT3 inhibitors based on BBI608

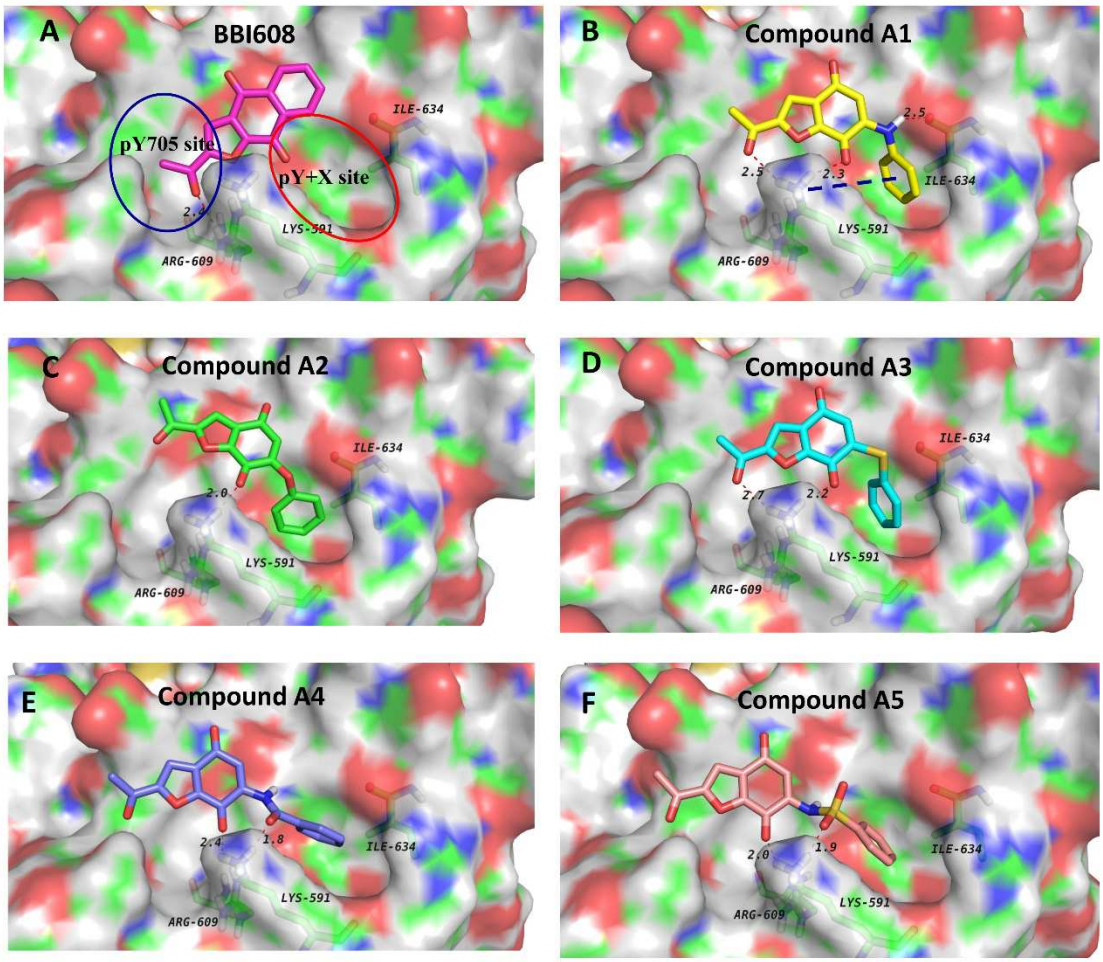


**Fig. 3.** Docking modes of BBI608 and designed compounds **A1**–**A5**.

## 2. Results and discussion

### 2.1 Chemistry

The synthetic route for designed compounds was described in Scheme 1. Upon treatment of commercially available, starting material **10** with bromine and aluminium trichloride, the electrophilic bromination of phenol occurred smoothly to deliver the dibromide **11** [43]. The *p*-bromophenol **11** was then easily oxidized to quinone **12** as a key intermediate by treatment of chromium oxide and acetic acid [43]. Finally, the target compounds were readily prepared through Pd-catalyzed C–N cross-coupling reaction with the use of various aromatic or aliphatic amines [44,45]. As a representative example, the exact structure of **A24** was unambiguously established by X-ray crystallography (Fig. 4) [46].

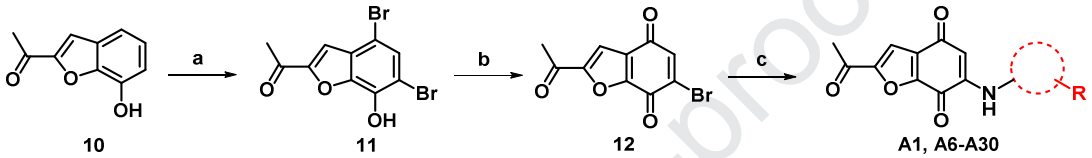


Regents and conditions: (a) $Br_2$, $AlCl_3$, $CH_2Cl_2$, 40 □; (b) $CrO_3$, $CH_3COOH$, 60 □; (c) $Pd(OAc)_2$, BINAP, $Cs_2CO_3$, Toluene, 120 □.

**Scheme 1.** Synthesis of Compounds **A1**, **A6-A30**

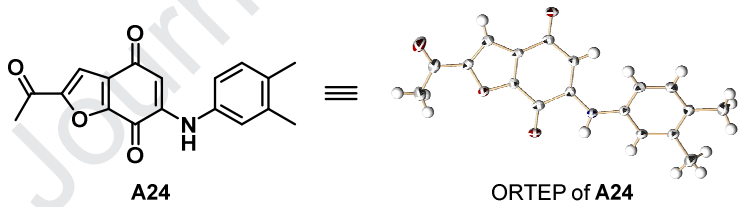


**Fig. 4.** X-ray crystallography of a representative compound **A24**.

## 2.2 Biological assay

### *2.2.1 In vitro cell growth inhibitory activity*

We firstly evaluated the inhibitory activities of our designed compounds against three STAT3 over-expressed human cancer cell lines (breast cancer cell lines: MDA-MB-231 and MDA-MB-468; human liver carcinoma cell line: HepG2) via established CCK8 assay. The $IC_{50}$ values were listed in Table 1 with BBI608 and Stattic as positive controls. In line with our expectations, all compounds displayed potent antiproliferative activities against tested cancer cells and their $IC_{50}$ values

ranged from sub-micromole to micromole. Apparently, compounds **A6** and **A11** exhibited considerable or even better inhibitory activities against two breast cancer cell lines compared to BBI608. The preliminary SAR that the additional functional groups occupied the side pocket was summarized as follows: Compound **A6** possessing a 2-$CH_3$ and compound **A11** containing a 4-$OCH_3$ showed better efficiency than other compounds with a single substituent group installed on the benzene ring (**A7**-**A10**, **A12**-**A20**). Incorporation of two or more substituents on the benzene ring (**A21**-**A25**) caused a slight decrease in activities. Changing phenyl substituent to different size of cycloalkyl substituents (**A26**-**A29**) led to the poor outcome that their corresponding derivatives except for cyclopropyl compound **A26** (0.94-1.97 μM**)** had relatively low potency. In addition, replacement of cyclohexyl group with tetrahydropyranyl substituent had no obvious effect on activities (compounds **A29** vs **A30**). Taken together, compound **A11** showed comprehensive potency *in vitro* anti-tumor activities and was selected for further biological study.

**Table 1.** Antiproliferative activity of the designed compounds

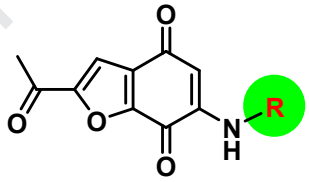


| Compd. | R | $IC_{50}$ ± SD (μM) [a] | | |
|---|---|---|---|---|
| | | MDA-MB-231 | MDA-MB-468 | HepG2 |
| **A1** | -Ph | 1.14±0.16 | 1.03±0.06 | 1.54±0.24 |
| **A6** | 2-$CH_3$-Ph | 0.56±0.10 | 0.73±0.04 | 1.21±0.01 |
| **A7** | 3-$CH_3$-Ph | 2.62±0.10 | 4.54±0.17 | 5.50±0.20 |
| **A8** | 4-$CH_3$-Ph | 0.90±0.08 | 3.12±0.02 | 1.85±0.07 |
| **A9** | 2-$OCH_3$-Ph | 0.92±0.08 | 1.05±0.11 | 2.41±0.33 |
| **A10** | 3-$OCH_3$-Ph | 1.48±0.06 | 1.55±0.05 | 2.36±0.33 |
| **A11** | 4-$OCH_3$-Ph | 0.67±0.02 | 0.77±0.01 | 1.24±0.16 |

| | | | | |
|---|---|---|---|---|
| **A12** | 2-F-Ph | 2.34±0.19 | 2.00±0.25 | 2.55±0.10 |
| **A13** | 3-F-Ph | 3.50±0.18 | 2.50±0.43 | 5.34±0.45 |
| **A14** | 4-F-Ph | 3.21±0.10 | 7.77±0.32 | 8.01±0.11 |
| **A15** | 2-$CF_3$-Ph | 3.12±0.23 | 1.75±0.12 | 4.04±0.21 |
| **A16** | 3-$CF_3$-Ph | 1.51±0.17 | 1.16±0.17 | 1.99±0.06 |
| **A17** | 4-$CF_3$-Ph | 3.70±0.30 | 2.27±0.50 | 6.17±0.13 |
| **A18** | 2-$C_2H_5$-Ph | 2.00±0.25 | 2.46±0.02 | 3.38±0.52 |
| **A19** | 4-$N(CH_3)_2$-Ph | 1.53±0.03 | 1.83±0.24 | 1.51±0.12 |
| **A20** | 4-isopropoxy-Ph | 1.11±0.19 | 1.18±0.25 | 1.04±0.18 |
| **A21** | 2-$CH_3$,4-$OCH_3$-Ph | 2.46±0.28 | 2.92±0.05 | 5.90±0.26 |
| **A22** | 2-$CH_3$,6-$CH_3$-Ph | 1.88±0.05 | 3.3±0.14 | 8.03±0.41 |
| **A23** | 2-$CH_3$,4-$OCH_3$,6-$CH_3$-Ph | 0.67±0.02 | 1.53±1.22 | 2.01±0.02 |
| **A24** | 3-$CH_3$,4-$CH_3$-Ph | 2.54±0.28 | 1.85±0.02 | 8.12±0.40 |
| **A25** | 3-$CH_3$,5-F-Ph | 2.62±0.37 | 2.11±0.26 | 5.66±0.46 |
| **A26** |  | 0.94±0.09 | 1.97±0.16 | 1.83±0.03 |
| **A27** |  | 4.87±0.20 | 8.84±0.64 | 6.75±0.06 |
| **A28** |  | 1.23±0.03 | 2.47±0.11 | 7.17±0.37 |
| **A29** |  | 2.88±0.07 | 4.13±0.44 | 6.55±0.18 |
| **A30** |  | 2.07±0.28 | 3.23±0.06 | 6.80±0.17 |
| BBI608 | - | 0.70±0.06 | 1.14±0.04 | 0.84±0.03 |
| Stattic | - | 2.64±0.03 | 1.92±0.08 | ND |

[a] The inhibitory effects of these compounds on the proliferation of cancer cell lines were determined by the CCK8 assay. The data are the mean ± SD from at least three independent experiments.

### *2.2.2 Fluorescence Polarization (FP) Assay*

It has been reported that STAT3 SH2 domain can bind to 5-FAM-GpYLPQTV-$NH_2$ derived peptide with a high affinity and then disrupted STAT3-STAT3 interaction and DNA-binding activity [47]. To verify the directly binding of the representative compounds **A6** and **A11** to the STAT3 SH2 domain, FP-based competition binding assay was conducted according to previously reported method (Fig. 5). Firstly, the 5-FAM-GpYLPQTV-$NH_2$derived peptide was applied as the fluorescent probe and showed the Kd value of 174 nM in our experiment, which was almost equivalent to the reported value (Kd=150 nM) by Berg and coworker [47]. Then, compound binding assays were performed in a 100 μL volume at a concentration of 10 nM 5-FAM-GpYLPQTV-$NH_2$ probe and 160 nM STAT3 protein. As demonstrated in Fig. 5, compounds **A6** and **A11** bound to STAT3 protein in a concentration-dependent manner with $IC_{50}$ values of 5.55 μM and 5.18 μM, respectively, which indicating the interaction of compounds **A6** and **A11** with the STAT3 SH2 domain.

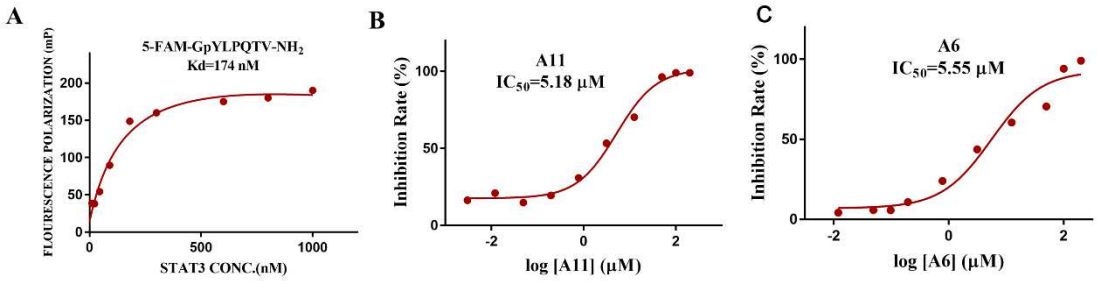


**Fig. 5.** (A) Binding of the fluorescent probes 5-FAM-GpYLPQTV-$NH_2$ to STAT3 SH2 domain. The probe was incubated at 10 nM with increasing amounts of STAT3 protein. (B) Dose−response competitive binding curve of compounds **A6** and **A11** to STAT3 using the FP-based binding assay.

### *2.2.3 Compounds **A11** and **A6** inhibited the phosphorylation of STAT3 and its downstream target proteins*

As STAT3 inhibitors can suppress the STAT3 phosphorylation on Tyr705 residue and thus restrain the expression of its downstream target proteins, then we turned our effort to the effects of compound **A11** and **A6** in MDA-MB-231 cells adopting western blot analysis. As shown in Fig. 6, compound **A11** and **A6** decreased the STAT3-Y705 phosphorylation in a dose-dependent manner without affecting the total

amount of STAT3 protein after 24 hrs incubation. These results clearly manifested that the decrease of Tyr705 phosphorylated STAT3 was not owing to the constitutional drop of total STAT3 protein, Also, these two representative compounds could decrease the expression of STAT3 target genes, including C-Myc and Cyclin D1, in a dose-dependent manner. It is noteworthy that compound **A11** and **A6** had little impact on the level of STAT1 and its phosphorylation on Tyr701, which suggested that they had a good selectivity against the tumor suppressor STAT1.

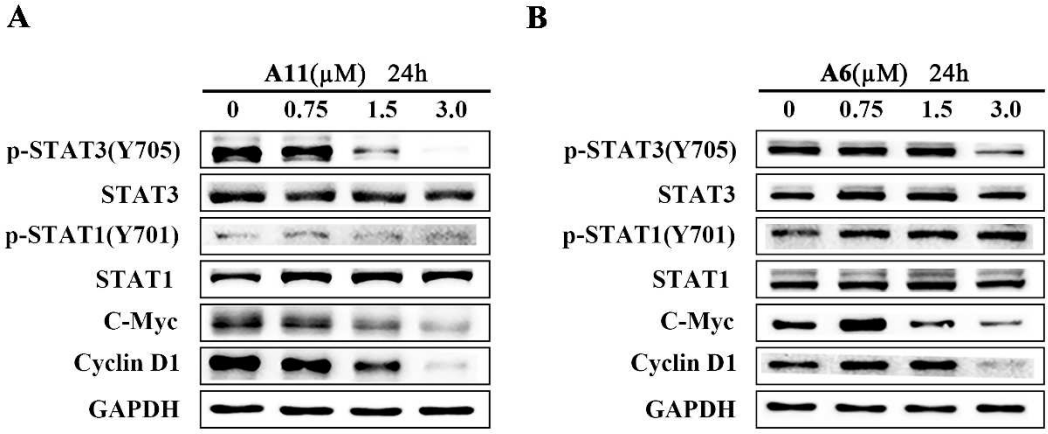


**Fig. 6.** Western blot analysis of the inhibition of STAT3-Y705 phosphorylation, the selective inhibition against STAT1 and the downstream target proteins (C-Myc and Cyclin D1) by compound **A11** in the MDA-MB-231 cell line. Cells were treated with **A11 or A6** for 24 hrs, and levels of STAT3, pSTAT3, STAT1, p-STAT1, C-Myc and Cyclin D1 were probed by specific antibodies. GAPDH was used as the loading control.

*2.2.4 Immunofluorescent assay*

To further explore the effect of compound **A11** on STAT3 phosphorylation in MDA-MB-231 cells, immunofluorescent assay was conducted. As expected, after incubation with MDA-MB-231 cells in 3.0 μM for 24 hrs, compound **A11** markedly reduced the expression of p-STAT3 (p-Tyr705) both in nucleus and cytoplasm compared to the control group (Fig. 7). The results provided another evidence that **A11** had an intense inhibition on the phosphorylation of STAT3 in MDA-MB-231 cells.

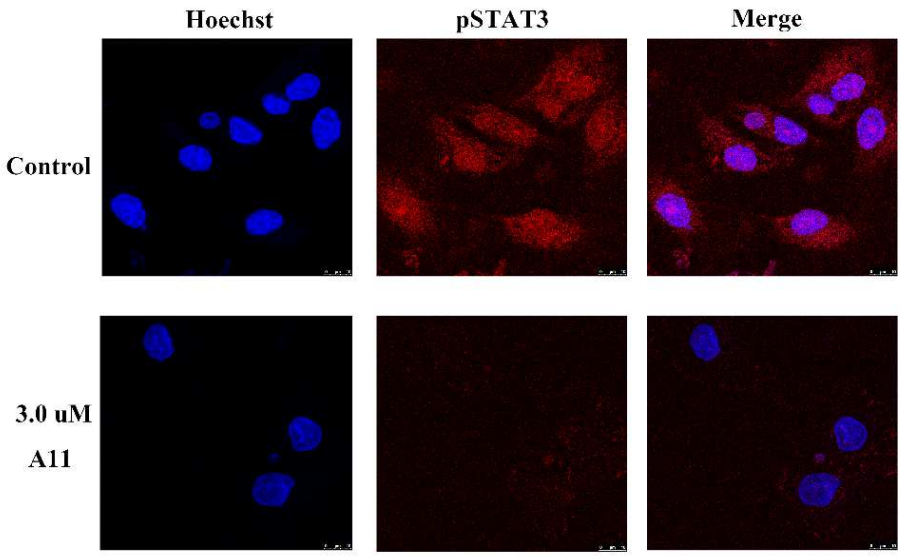


**Fig. 7.** MDA-MB-231 cells were incubated with 3.0 μM **A11** for 24 hrs and stained with anti-phospho-STAT3 (p-STAT3) and Hoechst before subjected to analysis. Red: p-STAT3; blue: nucleus (Scale bar: 10 μm).

*2.2.5 Compound **A11** induced apoptosis in cancer cells*

As we can see in Table 1, compound **A11** displayed potent anti-proliferative potency toward three cell lines, we then inquired the effect of **A11** in the induction of MDA-MB-231 cells apoptosis through Annexin-V-FITC/PI staining assay by flow cytometry. As depicted in Fig. 8, compound **A11** induced the apoptosis of MDA-MB-231 cell in a dose-dependent manner. The apoptosis rates at 0, 1, 2, 4 μM were 6.4%, 11.72%, 17.38%, and 32.28%, respectively, which was consistent with its antitumor efficacy in MDA-MB-231 cells.

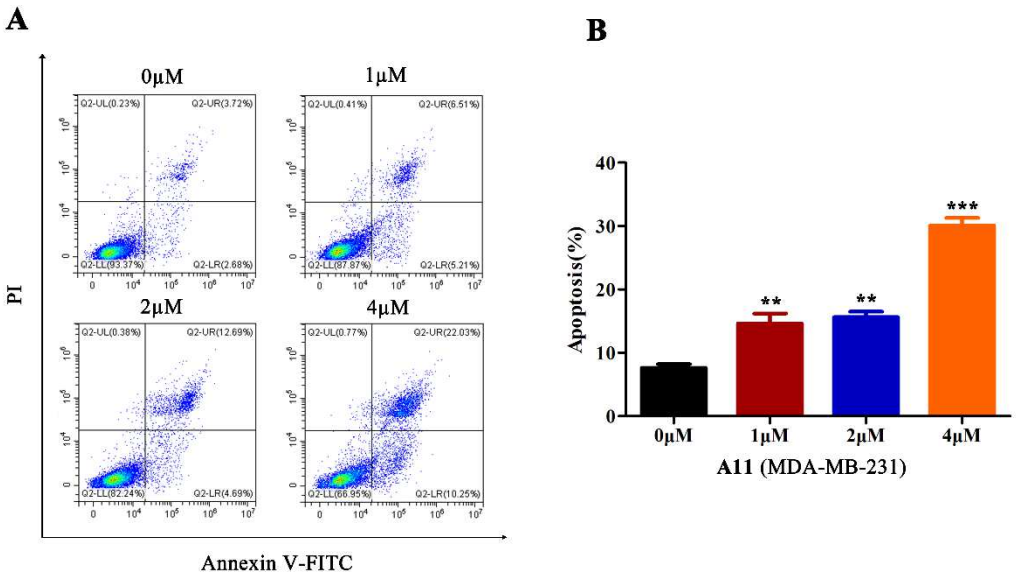


**Fig. 8.** Flow cytometric analysis of the apoptotic effect of compound **A11** in MDA-MB-231 cells through Annexin-V-FITC/PI staining assay. (A) MDA-MB-231 cells were treated with compound **A11** at tested concentrations for 24 h. (B) The histograms for apoptosis rate (early and late stages of apoptosis). Data are the mean ± SD of three independent experiments. ***, $p < 0.001$, **, $p < 0.01$.

*2.2.6 Analysis of cell cycle effect*

The effect of compound **A11** on cell cycle progression of MDA-MB-231 cells was assessed using flow cytometry and the results were shown in Fig. 9. After treating **A11** with MDA-MB-231 cells at the concentration of 0 μM, 1 μM, 2 μM and 4 μM for 24 hrs, the proportion of cells in S phase increased from 24.65 % to 53.40% accompanying with a decrease of cells in G0/G1 phase and G2/M phase. These results suggested that **A11** could dose-dependently cause a significant S phase arrest in MDA-MB-231 cells.

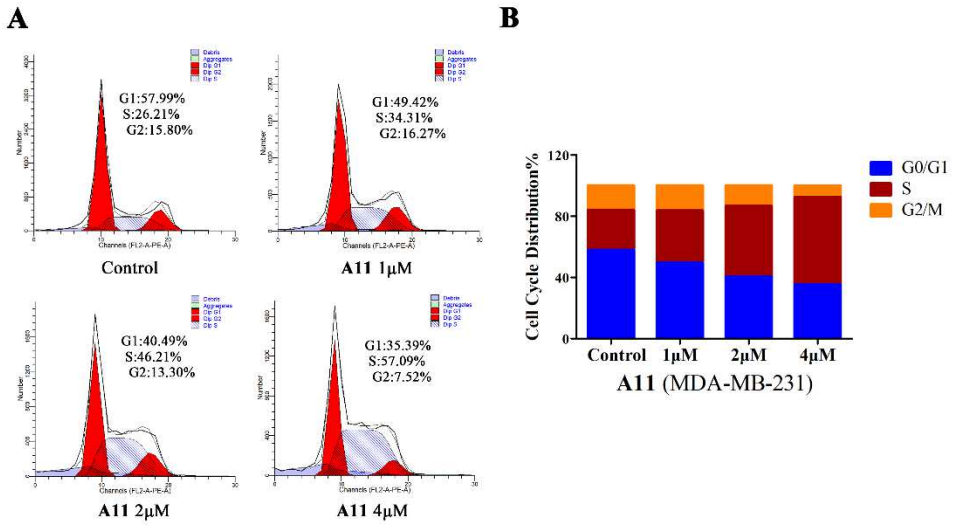


**Fig. 9.** Cell cycle analysis of compound **A11** by flow cytometry. MDA-MB-231 cells were treated with increasing concentrations of compound **A11** for 24 hrs.

*2.2.7 In Vivo Study of Compound **A11***

We then estimated the in *vivo* anti-tumor activity of compound **A11** using a mouse xenograft model bearing inoculation of human breast cancer cells MDA-MB-231. After the solid tumors were established, compound **A11** was intraperitoneally (i.p.) administered once daily at two doses (5 and 10 mg/kg) for 21 days. As demonstrated in Fig. 10A-B, the treatment with compound **A11** brought in an obvious reduction of the tumor volume at the dose of 10 mg/kg compared to control group on the twenty-first day ($TGI_{TV}$=54.62%). Besides, the tumor weights of mice were notably abated by 45.19% with a dosage of **A11** at 10 mg/kg (Fig. 10C). What's more, there was no apparent body-weight loss for those mice treated with compound **A11** at both dosage (Fig. 9D). Furthermore, the immunofluorescent assay of the tumor tissue revealed that the level of p-STAT3 (Y705) was obviously inhibited by compound **A11** at a dose of 10 mg/kg (Fig. 11). To sum up, compound **A11** exhibited good *in vivo* anti-tumor capacity and deserved further pharmaceutical studies.

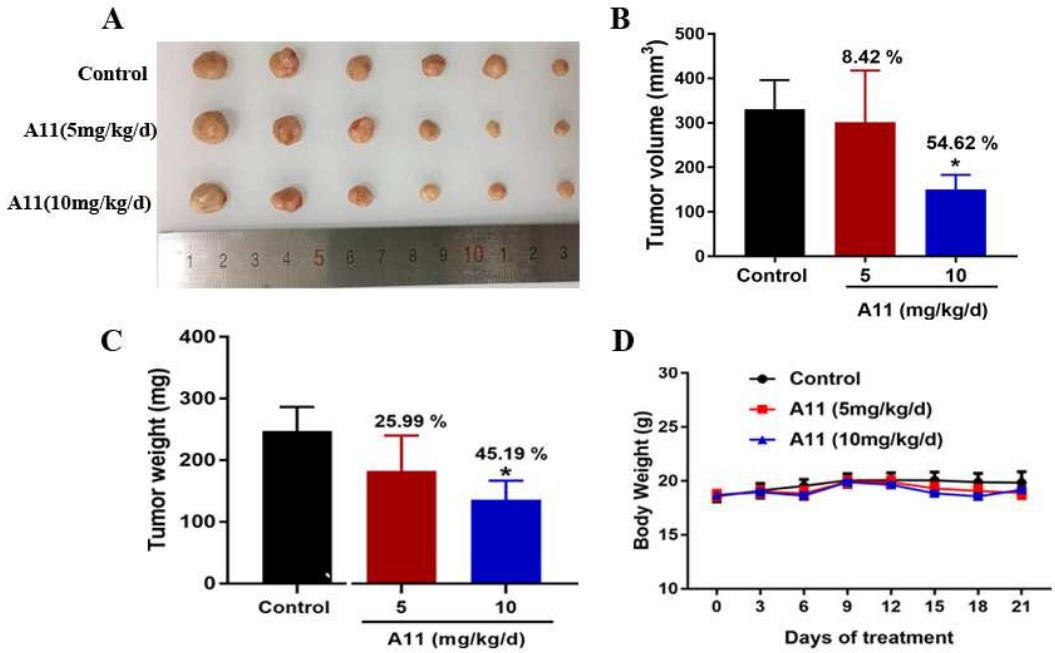


**Fig. 10.** Compound **A11** inhibited the growth of human xenograft tumor *in vivo*. MDA-MB-231 xenograft mouse models were treated with **A11** or vehicle control daily at indicated dosages for 21 consecutive days. (A) Anatomical nude mice's tumor tissues untreated or treated with **A11**. (B) The tumor volume and the tumor growth inhibition values ($TGI_{TV}$) were measured on the final day of the study. (C) The tumor weight and the tumor growth inhibition values ($TGI_{TW}$) were measured on the final day of the study. (D) The growing curves of mice's body weight. Data are shown as mean ± SEM, n=6; *, $P < 0.05$.

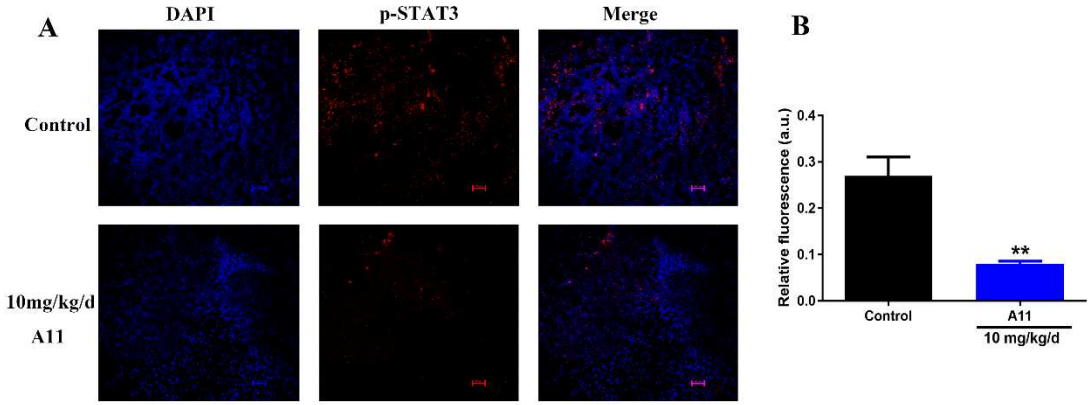


**Fig. 11.** Immunofluorescent assay revealed that **A11** inhibited the levels of p-STAT3 in tumor tissues. Data are shown as mean ± SEM, n=4; **, $p < 0.01$ (Scale bar: 50 μm).

*2.2.8 Molecular modeling simulations*

In an attempt to elucidate the binding mode of compound **A11** with STAT3 SH2 domain, docking study was carried out on the basis of the crystal structure of STAT3 homo dimer (PDB code: 1BG1). For a comparison, the binding mode of BBI608 was also generated and superimposed on that of **A11** (Fig. 12A). As represented, the p-methoxyphenyl in compound **A11** was extended to the pY+X site, which was not occupied by BBI608 as expected. Such a transformation subsequently gained a hydrogen bond interaction between the methoxy group of **A11** and the guanidyl of ARG595. Moreover, the NH formed a strong hydrogen bond with ILE634 and the distance was 2.0 Å. The other one hydrogen bond (2.5 Å) was engendered between the oxygen atom of acetyl and the amino group of LYS591. (Fig. 12B) In general, all these interactions ensured the activities of compound **A11** toward STAT3 protein.

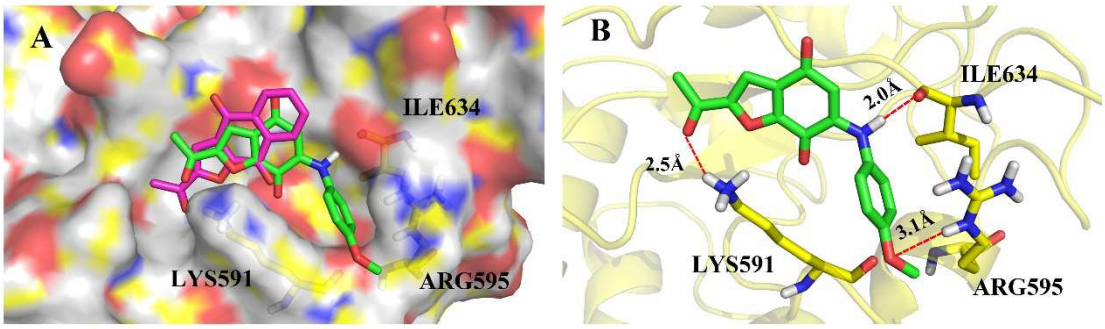


**Fig. 12.** Molecular modeling study of **A11** in STAT3 SH2 domain (PDB code: 1BG1). (A) Superimposed pose of **A11** (green) and BBI606 (pink) bound in the surface of binding site. (B) Predicted interaction of **A11** (green) within STAT3 SH2 domain. The figures were generated using Pymol.

## 3. Conclusions

In summary, structure-based drug design strategy was applied to generate new scaffold STAT3 inhibitors based on BBI608. Among them, compound **A11** was evinced to be remarkable anti-tumor activities against MDA-MB-231, MDA-MB-468 and HepG2 cells *in vitro* with an $IC_{50}$ range of 0.67−1.24 μM. The direct interaction between compound **A11** and STAT3 SH2 domain was validated using fluorescence polarization assay with the $IC_{50}$ value of 5.18 μM. Cellular mechanistic studies

showed that **A11** can suppress the expression level of phosphorylated STAT3 (p-STAT3) and then downregulated its downstream gene C-Myc and Cyclin D1 without influence the total STAT3 protein. Furthermore, compound **A11** manifested good selectivity against STAT1 which was a member of STAT family and a tumor suppressor. Moreover, **A11** displayed preferable anti-tumor efficacy *in vivo* toward MDA-MB-231 xenograft mouse model at a low dose of 10 mg/kg. Finally, molecular docking study clarified the binding mode of compound **A11** in STAT3 SH2 domain. Collectively, these studies provided more structural reference for the development of STAT3 inhibitors and suggested that compound **A11** might be a highly potent and minimally toxic anti-tumor lead compound worthy of further investigation.

## 4. Experimental section

### *4.1. Chemistry*

All solvents and reagents were purchased from commercial suppliers such as Bide pharmatech, Adamas-beta®, etc., and directly used without further purification unless specified. Flash chromatography was performed on silica gel (200-300 mesh) and visualized under UV light monitor ($\lambda$ = 254 nm and 365 nm). The nuclear magnetic resonance (NMR) spectroscopy were recorded in $CDCl_3$ or DMSO-$d_6$ with Bruker 600 MHz spectrometer (TMS as internal standard) at ambient temperature. The chemical shifts ($\delta$) were expressed in parts per million (ppm) downfield and coupling constants ($J$) values were described as hertz. MS was measured on Shimadzu 8040 quadrupole LC/MS system. High-resolution mass spectra (HRMS) data were given by Agilent 6545 Accurate-Mass Q-TOF LC/MS system. The X-Ray crystal structures of compound **A24** was measured on X-ray Single Crystal Diffractometer (Bruker D8 Venture).

#### *4.1.1. Synthesis of 1-(4,6-dibromo-7-hydroxybenzofuran-2-yl)ethan-1-one* (**11**)

To a solution of 1-(7-hydroxybenzofuran-2-yl)ethan-1-one (**10**, 5.0 g, 28.29 mmol) in $CH_2Cl_2$ (200 mL) was added $AlCl_3$ (15.1 g, 113.24 mmol) and the mixture was keeping stirred for 1 h at 40 □. Then, $Br_2$ (10.0 g, 62.57 mmol) was added dropwise

to the reaction mixture over 90 min period at 26 □. The resulting mixture was stirred for 18 hrs at 26 □, and poured into ice water, and followed by treatment of sodium thiosulfate. The resulting precipitate was collected by filtration and washed with water, then recrystallized from ethyl acetate to give the compound **11**. Colorless solid; yield: 93.1%. $^1$H NMR (600 MHz, DMSO-$d_6$) $\delta$ 11.40 (s, 1H)，7.86 (s, 1H), 7.72 (s, 1H), 2.61 (s, 3H). ESI-LCMS $[M+H]^+$ calcd for $C_{10}H_7Br_2O_3$ 332.88, found: 332.75.

*4.1.2. Synthesis of 2-acetyl-6-bromobenzofuran-4,7-dione* (**12**)

To a solution of compound **11** (8.8 g, 26.28 mmol) in 100 mL of 80 % acetic acid in water was added $CrO_3$ (5.8 g, 52.56 mmol, a solution in 20 mL of water). The reaction mixture was stirred at room temperature for 3 hrs. After cooling to room temperature, the reaction solution was concentrated in *vacuo* and the residue was dissolved in chloroform. The chloroform phase was washed with water, dried over sodium sulfate, and concentrated in *vacuo*. The residue was purified by column chromatography (PE/EA = 4:1) to give the compound **12**. Yellow solid; yield: 34.5%. $^1$H NMR (600 MHz, $CDCl_3$) $\delta$ 7.46 (s, 1H)，7.34 (s, 1H)，2.64 (s, 3H). ESI-LCMS $[M+H]^+$ calcd for $C_{10}H_6BrO_4$ 268.94, found: 268.85.

*4.1.3. Synthesis of compounds **A1**, **A6-A30***

To a Schlenk flask was added the corresponding amine (0.20 mmol), 2-acetyl-6-bromobenzofuran-4,7-dione (**12**, 60.0 mg, 0.22 mmol), $Pd(OAc)_2$ (5.5 mg, 0.02 mmol), BINAP (14.3 mg, 0.02 mmol), $Cs_2CO_3$ (293.2 mg, 0.9 mmol) and anhydrous toluene (6.0 mL) under nitrogen atmosphere, respectively. The reaction mixture was refluxed at 120 °C for 8 hrs. After cooling to room temperature, the mixture was filtered through a pad of Celite and washed with ethyl acetate. The organic solvent was removed under vacuum and the residue was purified by silica-gel column chromatography to give the compounds **A1**, **A6-A30**.

*4.1.3.1. 2-Acetyl-6-(phenylamino)benzofuran-4,7-dione* (**A1**)

Purple solid; yield: 32.3%. $^1$H NMR (600 MHz, $CDCl_3$) $\delta$ 7.46 (d, $J$ = 4.2 Hz, 2H), 7.43 (d, $J$ = 7.8 Hz, 2H), 7.27 (s, 1H), 7.26 (d, $J$ = 3.8 Hz, 2H), 6.17 (s, 1H), 2.64 (s, 3H). $^{13}$C NMR (150 MHz, $CDCl_3$) $\delta$ 187.30, 180.63, 171.62, 155.97, 149.09, 144.46,

137.02, 131.53, 129.82, 126.22, 122.85, 112.53, 100.66, 26.71. ESI-HRMS $[M+H]^+$ calcd for $C_{16}H_{12}NO_4$ 282.0761, found: 282.0768.

*4.1.3.2. 2-Acetyl-6-(o-tolylamino)benzofuran-4,7-dione* (**A6**)

Purple solid; yield: 23.2%, $^1$H NMR (600 MHz, $CDCl_3$) $\delta$ 7.45 (s, 1H), 7.31 (d, $J$ = 7.5 Hz, 1H), 7.28 (s, 1H), 7.25-7.22 (m, 3H), 5.70 (s, 1H), 2.63 (s, 3H), 2.28 (s, 3H). $^{13}$C NMR (150 MHz, DMSO-$d_6$) $\delta$ 187.54, 180.08, 171.97, 155.10, 150.36, 148.56, 136.65, 135.10, 131.56, 130.66, 127.89, 127.40, 127.30, 114.64, 99.06, 27.12, 17.86. ESI-HRMS $[M+Na]^+$ calcd for $C_{17}H_{13}NNaO_4$ 318.0737, found: 318.0754.

*4.1.3.3. 2-Acetyl-6-(m-tolylamino)benzofuran-4,7-dione* (**A7**)

Purple solid; yield: 36.6%, $^1$H NMR (600 MHz, $CDCl_3$) $\delta$ 7.46 (s, 1H), 7.42 (s, 1H), 7.31 (t, $J$ = 7.4 Hz, 1H), 7.06 (d, $J$ = 10.9 Hz, 3H), 6.17 (s, 1H), 2.63 (s, 3H), 2.39 (s, 3H). $^{13}$C NMR (150 MHz, $CDCl_3$) $\delta$ 187.31, 180.66, 171.67, 155.97, 149.10, 144.48, 139.97, 136.94, 131.57, 129.62, 127.04, 123.33, 119.85, 112.54, 100.62, 26.70, 21.44. ESI-HRMS $[M+Na]^+$ calcd for $C_{17}H_{13}NNaO_4$ 318.0737, found: 318.0745.

*4.1.3.4. 2-Acetyl-6-(p-tolylamino)benzofuran-4,7-dione* (**A8**)

Purple solid; yield: 35.4%, $^1$H NMR (600 MHz, $CDCl_3$) $\delta$ 7.45 (s, 1H), 7.41 (s, 1H), 7.23 (d, $J$ = 8.1 Hz, 2H), 7.15 (d, $J$ = 8.2 Hz, 2H), 6.10 (s, 1H), 2.63 (s, 3H), 2.37 (s, 3H). $^{13}$C NMR (150 MHz, $CDCl_3$) $\delta$ 187.31, 180.54, 171.69, 155.94, 149.10, 144.76, 136.31, 134.34, 131.62, 130.36, 122.90, 112.56, 100.29, 26.69, 21.03. ESI-HRMS $[M+Na]^+$ calcd for $C_{17}H_{13}NNaO_4$ 318.0737, found: 318.0744.

*4.1.3.5. 2-Acetyl-6-((2-methoxyphenyl)amino)benzofuran-4,7-dione* (**A9**)

Purple solid ; yield: 30.8%, $^1$H NMR (600 MHz, $CDCl_3$) $\delta$ 7.87 (s, 1H), 7.46 (s, 1H), 7.40-7.38 (m, 1H), 7.20-7.16 (m, 1H), 7.02 (t, $J$ = 7.5 Hz, 1H), 6.98 (d, $J$ = 8.2 Hz, 1H), 6.24 (s, 1H), 3.93 (s, 3H), 2.63 (s, 3H). $^{13}$C NMR (150 MHz, $CDCl_3$) $\delta$ 187.35, 180.68, 171.70, 155.84, 151.27, 149.24, 143.62, 131.45, 126.44, 126.13, 121.34, 120.92, 112.52, 111.23, 100.79, 55.79, 26.71. ESI-HRMS $[M+H]^+$ calcd for $C_{17}H_{14}NO_5$ 312.0866, found: 312.0859.

*4.1.3.6. 2-Acetyl-6-((3-methoxyphenyl)amino)benzofuran-4,7-dione* (**A10**)

Purple solid; yield: 32.2%, $^1$H NMR (600 MHz, $CDCl_3$) $\delta$ 7.46 (s, 1H), 7.42 (s, 1H), 7.35-7.32 (m, 1H), 6.85 (d, $J$ = 7.4 Hz, 1H), 6.79-6.78(m, 2H), 6.21 (s, 1H), 3.83 (s,

3H), 2.63 (s, 3H). $^{13}$C NMR (150 MHz, $CDCl_3$) $\delta$ 187.28, 180.63, 171.61, 160.69, 155.98, 149.09, 144.30, 138.19, 131.51, 130.60, 114.97, 112.52, 111.51, 108.76, 101.09, 55.48, 26.69. ESI-HRMS $[M+H]^+$ calcd for $C_{17}H_{14}NO_5$ 312.0866, found: 312.0866.

*4.1.3.7. 2-Acetyl-6-((4-methoxyphenyl)amino)benzofuran-4,7-dione* (**A11**)

Purple solid; yield: 15.1%, $^1$H NMR (600 MHz, $CDCl_3$) $\delta$ 7.45 (s, 1H), 7.35 (s, 1H), 7.19 (d, $J$ = 8.9 Hz, 2H), 6.95 (d, $J$ = 8.9 Hz, 2H), 5.98 (s, 1H), 3.84 (s, 3H), 2.63 (s, 3H). $^{13}$C NMR (150 MHz, $CDCl_3$) $\delta$ 187.31, 180.42, 171.68, 158.03, 155.94, 149.11, 145.41, 131.72, 129.59, 124.97, 115.01, 112.58, 99.83, 55.58, 26.69. ESI-HRMS $[M+H]^+$ calcd for $C_{17}H_{14}NO_5$ 312.0866, found: 312.0867.

*4.1.3.8. 2-Acetyl-6-((2-fluorophenyl)amino)benzofuran-4,7-dione* (**A12**)

Purple solid; yield: 27.5%, $^1$H NMR (600 MHz, $CDCl_3$) $\delta$ 7.46 (s, 1H), 7.41-7.39 (m, 2H), 7.24-7.21 (m, 3H), 6.05 (s, 1H), 2.64 (s, 3H). $^{13}$C NMR (150 MHz, $CDCl_3$) $\delta$ 187.31, 180.62, 171.26, 156.03, 154.65, 149.15, 144.18, 131.35, 127.32, 125.29, 124.92, 124.07, 116.74, 112.44, 101.85, 26.71. ESI-HRMS $[M+H]^+$ calcd for $C_{16}H_{11}FNO_4$ 300.0667, found: 300.0679.

*4.1.3.9. 2-Acetyl-6-((3-fluorophenyl)amino)benzofuran-4,7-dione* (**A13**)

Purple solid; yield: 15.7%, $^1$H NMR (600 MHz, $CDCl_3$) $\delta$ 7.46 (s, 1H), 7.43 (s, 1H), 7.40 (d, $J$ = 6.8 Hz, 1H), 7.05 (d, $J$ = 7.7 Hz, 1H), 7.01 (d, $J$ = 9.4 Hz, 1H), 6.95 (t, $J$ = 7.7 Hz, 1H), 6.21 (s, 1H), 2.64 (s, 3H). $^{13}$C NMR (150 MHz, $CDCl_3$) $\delta$ 187.27, 180.65, 171.38, 164.11, 162.46, 156.07, 149.06, 143.86, 138.67, 131.13, 118.23, 112.94, 112.50, 109.83, 101.60, 26.72. ESI-HRMS $[M-H]^-$ calcd for $C_{16}H_9FNO_4$ 298.0516, found: 298.0517.

*4.1.3.10. 2-Acetyl-6-((4-fluorophenyl)amino)benzofuran-4,7-dione* (**A14**)

Purple solid; yield: 15.3%, $^1$H NMR (600 MHz, $CDCl_3$) $\delta$ 7.49 (s, 1H), 7.45 (s, 1H), 7.25-7.23 (m, 2H), 7.15 (t, $J$ = 8.4 Hz, 2H), 6.01 (s, 1H), 2.62 (s, 3H). $^{13}$C NMR (150 MHz, $CDCl_3$) $\delta$ 187.26, 175.92, 168.99, 161.90, 160.26, 155.02, 152.69, 143.62, 132.83, 127.12, 124.78, 115.68, 115.53, 111.55, 102.64, 26.73. ESI-HRMS $[M+H]^+$ calcd for $C_{16}H_{11}FNO_4$ 300.0667, found: 300.0675.

*4.1.3.11. 2-Acetyl-6-((2-(trifluoromethyl)phenyl)amino)benzofuran-4,7-dione* (**A15**)

Orange solid; yield: 35.8%, $^{1}$H NMR (600 MHz, $CDCl_3$) $\delta$ 7.76 (d, $J$ = 7.9 Hz, 1H), 7.65 (t, $J$ = 7.6 Hz, 1H), 7.51 (d, $J$ = 8.0 Hz, 1H), 7.49 (s, 1H), 7.46 (s, 1H), 7.41 (t, $J$ = 7.5 Hz, 1H), 5.94 (s, 1H), 2.64 (s, 3H). $^{13}$C NMR (150 MHz, $CDCl_3$) δ 187.34, 180.65, 171.02, 156.06, 149.06, 145.13, 135.18, 133.15, 131.32, 127.45, 127.42, 126.72, 126.25, 112.36, 101.67, 26.71. ESI-HRMS $[M+H]^+$ calcd for $C_{17}H_{11}F_3NO_4$ 350.0635,found: 350.0632.

*4.1.3.12. 2-Acetyl-6-((3-(trifluoromethyl)phenyl)amino)benzofuran-4,7-dione* (**A16**)

Purple solid; yield: 29.9%, $^{1}$H NMR (600 MHz, $CDCl_3$) $\delta$ 7.60-7.56 (m, 1H), 7.51 (s, 2H), 7.48 (d, $J$ = 7.3 Hz, 3H), 6.16 (s, 1H), 2.64 (s, 3H). $^{13}$C NMR (150 MHz, $CDCl_3$) $\delta$ 187.25, 180.60, 171.25, 156.13, 149.01, 143.93, 137.82, 131.43, 130.54, 125.78, 122.73, 122.70, 119.57, 119.55, 112.48, 101.55, 26.73. ESI-HRMS $[M+H]^+$ calcd for $C_{17}H_{11}F_3NO_4$ 350.0635, found: 350.0630.

*4.1.3.13. 2-Acetyl-6-((4-(trifluoromethyl)phenyl)amino)benzofuran-4,7-dione* (**A17**)

Red solid; yield: 39.1%, $^{1}$H NMR (600 MHz, $CDCl_3$) $\delta$ 7.76 (d, $J$ = 7.8 Hz, 1H), 7.65 (t, $J$ = 7.7 Hz, 1H), 7.51 (d, $J$ = 8.0 Hz, 1H), 7.49 (s, 1H), 7.45 (s, 1H), 7.41 (t, $J$ = 7.7 Hz, 1H), 5.94 (s, 1H), 2.64 (s, 3H). $^{13}$C NMR (150 MHz, $CDCl_3$) $\delta$ 187.35, 180.66, 171.03, 156.08, 149.08, 145.14, 135.19, 133.17, 131.34, 127.44, 126.74, 126.27, 112.38, 101.69, 26.73. ESI-HRMS $[M+H]^+$ calcd for $C_{17}H_{11}F_3NO_4$ 350.0635, found: 350.0638.

*4.1.3.14. 2-Acetyl-6-((2-ethylphenyl)amino)benzofuran-4,7-dione* (**A18**)

Purple solid; yield: 24.4%, $^{1}$H NMR (600 MHz, $CDCl_3$) $\delta$ 7.50 (s, 1H), 7.37 (s, 1H), 7.35-7.33 (m, 1H), 7.29-7.28 (m, 2H), 7.25-7.23 (m, 1H), 5.75 (s, 1H), 2.63-2.60 (m, 5H), 1.22 (t, $J$ = 7.6 Hz, 3H). $^{13}$C NMR (150 MHz, $CDCl_3$) $\delta$ 187.38, 175.97, 169.02, 154.90, 153.03, 144.12, 139.73, 135.09, 128.80, 127.82, 127.12, 125.92, 124.59, 111.60, 101.26, 26.77, 24.82, 13.87. ESI-HRMS $[M-H]^-$ calcd for $C_{18}H_{14}NO_4$ 308.0923, found: 308.0933.

*4.1.3.15. 2-Acetyl-6-((4-(dimethylamino)phenyl)amino)benzofuran-4,7-dione* (**A19**)

Purple solid; yield: 65.5%, $^{1}$H NMR (600 MHz, $CDCl_3$) $\delta$ 7.56 (s, 1H), 7.48 (s, 1H), 7.14 (d, $J$ = 8.8 Hz, 2H), 6.73 (d, $J$ = 8.8 Hz, 2H), 6.05 (s, 1H), 3.00 (s, 6H), 2.62 (s, 3H).$^{13}$C NMR (150 MHz, $CDCl_3$) $\delta$ 187.63, 178.41, 174.93, 155.01, 154.34, 149.08,

146.00, 125.33, 124.44, 124.30, 112.83, 111.49, 98.88, 40.52, 26.72. ESI-HRMS $[M+H]^+$ calcd for $C_{18}H_{17}N_2O_4$ 325.1183, found: 325.1169.

*4.1.3.16. 2-Acetyl-6-((4-isopropoxyphenyl)amino)benzofuran-4,7-dione* (**A20**)

Purple solid; yield: 21.7%, $^1$H NMR (600 MHz, $CDCl_3$) $\delta$ 7.48 (s, 1H), 7.46 (s, 1H), 7.16 (d, $J$ = 8.8 Hz, 2H), 6.93 (d, $J$ = 8.8 Hz, 2H), 6.02 (s, 1H), 4.58-4.54 (m, 1H), 2.62 (s, 3H), 1.36 (s, 3H), 1.35 (s, 3H). $^{13}$C NMR (150 MHz, $CDCl_3$) $\delta$ 187.42, 178.26, 175.16, 156.57, 154.60, 154.49, 146.23, 129.11, 124.98, 124.47, 116.89, 111.40, 99.43, 70.43, 26.69, 21.97. ESI-HRMS $[M+H]^+$ calcd for $C_{19}H_{18}NO_5$ 340.1179, found: 340.1165.

*4.1.3.17. 2-Acetyl-6-((4-methoxy-2-methylphenyl)amino)benzofuran-4,7-dione* (**A21**)

Purple solid; yield: 22.2%, $^1$H NMR (600 MHz, $CDCl_3$) $\delta$ 7.42 (s, 1H), 7.18 (s, 1H), 7.06 (d, $J$ = 8.4 Hz, 1H), 6.76 (s, 1H), 6.73 (d, $J$ = 8.2 Hz, 1H), 5.51 (s, 1H), 3.75 (s, 3H), 2.55 (s, 3H), 2.16 (s, 3H). $^{13}$C NMR (150 MHz, $CDCl_3$) $\delta$ 187.38, 175.96, 169.02, 159.02, 154.83, 153.22, 144.26, 136.43, 128.45, 128.39, 124.40, 115.55, 111.57, 111.24, 100.05, 55.44, 26.77, 18.66. ESI-HRMS $[M+H]^+$ calcd for $C_{18}H_{16}NO_5$ 326.1023, found: 326.1021.

*4.1.3.18. 2-Acetyl-6-((2,6-dimethylphenyl)amino)benzofuran-4,7-dione* (**A22**)

Red solid; yield: 11.5%, $^1$H NMR (600 MHz, $CDCl_3$) $\delta$ 7.49 (s, 1H), 7.25 (s, 1H), 7.13 (d, $J$ = 8.6 Hz, 1H), 6.83 (s, 1H), 6.80 (dd, $J$ = 8.6, 2.3 Hz, 1H), 5.58 (s, 1H), 3.82 (s, 3H), 2.62 (s, 3H), 2.23 (s, 3H). $^{13}$C NMR (150 MHz, $CDCl_3$) $\delta$ 187.61, 178.26, 175.09, 158.88, 154.70, 154.48, 147.42, 135.45, 127.50, 126.82, 124.55, 116.63, 112.45, 111.40, 99.55, 55.52, 26.72, 18.02. ESI-HRMS $[M+Na]^+$ calcd for $C_{18}H_{15}NNaO_4$ 332.0893, found: 332.0892.

*4.1.3.19. 2-Acetyl-6-((4-methoxy-2,6-dimethylphenyl)amino)benzofuran-4,7-dione* (**A23**)

Purple solid; yield: 25.6%, $^1$H NMR (600 MHz, $CDCl_3$) $\delta$ 7.43 (s, 1H), 6.93 (s, 1H), 6.67 (s, 2H), 5.14 (s, 1H), 3.80 (s, 3H), 2.63 (s, 3H), 2.17 (s, 6H). $^{13}$C NMR (150 MHz, $CDCl_3$) $\delta$ 187.34, 180.21, 171.61, 159.09, 155.91, 149.28, 146.99, 136.97, 131.90, 126.02, 113.99, 113.97, 112.64, 99.96, 55.39, 26.68, 18.28. ESI-HRMS $[M+H]^+$ calcd for $C_{19}H_{18}NO_5$ 340.1179, found: 340.1179.

*4.1.3.20. 2-acetyl-6-((3,4-dimethylphenyl)amino)benzofuran-4,7-dione* (**A24**)

Purple solid; yield: 26.1%, $^{1}$H NMR (600 MHz, $CDCl_3$) $\delta$ 7.45 (s, 1H), 7.40 (s, 1H), 7.17 (d, $J$ = 8.0 Hz, 1H), 7.03 (s, 1H), 6.99 (d, $J$ = 8.0 Hz, 1H), 6.12 (s, 1H), 2.63 (s, 3H), 2.28 (s, 3H), 2.27 (s, 3H). $^{13}$C NMR (150 MHz, $CDCl_3$) $\delta$ 187.32, 180.57, 171.73, 155.93, 149.10, 144.74, 138.35, 135.02, 134.58, 131.65, 130.76, 123.99, 120.27, 112.56, 100.22, 26.69, 19.93, 19.36. ESI-HRMS $[M+H]^+$ calcd for $C_{18}H_{16}NO_4$ 310.1074, found: 310.1083.

*4.1.3.21. 2-Acetyl-6-((3-fluoro-5-methylphenyl)amino)benzofuran-4,7-dione* (**A25**)

Purple solid; yield: 22.2%, $^{1}$H NMR (600 MHz, $CDCl_3$) $\delta$ 7.61 (s, 1H), 7.48 (s, 1H), 6.79 (d, $J$ = 9.2 Hz, 1H), 6.69 (s, 1H), 6.62 (d, $J$ = 9.1 Hz, 1H), 2.64 (s, 3H), 2.36 (s, 3H).$^{13}$C NMR (150 MHz, $CDCl_3$) $\delta$ 187.26, 175.92, 169.00, 163.22, 155.06, 152.50, 143.30, 140.48, 137.79, 124.98, 121.10, 113.94, 111.58, 109.14, 104.38, 26.75, 21.46. ESI-HRMS $[M+H]^+$ calcd for $C_{17}H_{13}FNO_4$ 314.0823, found: 314.0834.

*4.1.3.22. 2-Acetyl-6-(cyclopropylamino)benzofuran-4,7-dione* (**A26**)

Red solid; yield: 39.1%, $^{1}$H NMR (600 MHz, $CDCl_3$) $\delta$ 7.42 (s, 1H), 6.08 (s, 1H), 5.88 (s, 1H), 2.61 (s, 3H), 2.52 (m, 1H), 0.93 (d, J = 6.7 Hz, 2H), 0.69 (s, 2H). $^{13}$C NMR (150 MHz, $CDCl_3$) $\delta$ 187.57, 177.91, 174.71, 154.75, 154.34, 149.74, 124.59, 111.35, 99.82, 26.69, 24.55, 7.26. ESI-HRMS $[M+H]^+$ calcd for $C_{13}H_{12}NO_4$ 246.0761, found: 246.0766.

*4.1.3.23. 2-Acetyl-6-(cyclobutylamino)benzofuran-4,7-dione* (**A27**)

Red solid; yield: 26.3%, $^{1}$H NMR (600 MHz, $CDCl_3$) $\delta$ 7.43 (s, 1H), 6.12 (s, 1H), 5.40 (s, 1H), 3.92 (dd, $J$ = 14.2, 7.0 Hz, 1H), 2.60 (s, 3H), 2.49 (d, $J$ = 7.4 Hz, 2H), 2.05-2.02 (m, 2H), 1.94-1.88 (m, 2H). $^{13}$C NMR (150 MHz, $CDCl_3$) $\delta$ 187.58, 177.91, 174.45, 154.96, 154.29, 147.25, 124.36, 111.38, 98.31, 47.96, 29.92, 26.69, 15.63. ESI-HRMS $[M+H]^+$ calcd for $C_{14}H_{14}NO_4$ 260.0917, found: 260.0906.

*4.1.3.24. 2-Acetyl-6-(cyclopentylamino)benzofuran-4,7-dione* (**A28**)

Purple solid; yield: 6.2%, $^{1}$H NMR (600 MHz, $CDCl_3$) $\delta$ 7.43 (s, 1H), 5.98 (d, $J$ = 4.6 Hz, 1H), 5.53 (s, 1H), 3.80-3.74 (m, 1H), 2.60 (s, 3H), 2.10-2.05 (m, 2H), 1.77-1.64 (m, 6H). $^{13}$C NMR (150 MHz, $CDCl_3$) $\delta$ 187.59, 177.97, 174.34, 155.09, 154.28,

148.08, 124.28, 111.41, 98.29, 54.43, 32.71, 26.69, 24.10. ESI-HRMS $[M+H]^+$ calcd for $C_{15}H_{16}NO_4$ 274.1074, found: 274.1076.

*4.1.3.25. 2-Acetyl-6-(cyclohexylamino)benzofuran-4,7-dione* (**A29**)

Purple solid; yield: 25.7%, $^1$H NMR (600 MHz, $CDCl_3$) $\delta$ 7.43 (s, 1H), 5.96 (d, $J$ = 5.2 Hz, 1H), 5.53 (s, 1H), 3.30-3.25 (m, 1H), 2.60 (s, 3H), 2.03 (d, $J$ = 11.4 Hz, 2H), 1.82-1.80 (m, 2H), 1.70-1.68 (m, 2H), 1.39-1.31 (m, 4H).$^{13}$C NMR (150 MHz, $CDCl_3$) $\delta$ 187.62, 178.06, 174.48, 155.11, 154.28, 147.45, 124.32, 111.42, 97.69, 51.94, 31.73, 26.70, 25.34, 24.49. ESI-HRMS $[M+H]^+$ calcd for $C_{16}H_{18}NO_4$ 287.1230, found: 288.1220.

*4.1.3.26. 2-Acetyl-6-((tetrahydro-2H-pyran-4-yl)amino)benzofuran-4,7-dione* (**A30**)

Red solid; yield: 35.3%, $^1$H NMR (600 MHz, $CDCl_3$) $\delta$ 7.37 (s, 1H), 5.84 (s, 1H), 5.48 (s, 1H), 3.96 (d, $J$ = 10.8 Hz, 2H), 3.44 (t, $J$ = 10.6 Hz, 3H), 2.54 (s, 3H), 1.96 (d, $J$ = 12.3 Hz, 2H), 1.57 (d, $J$ = 10.6 Hz, 2H).$^{13}$C NMR (150 MHz, $CDCl_3$) $\delta$ 187.54, 177.84, 174.56, 154.70, 154.38, 147.09, 124.48, 111.41, 98.13, 66.23, 49.25, 31.75, 26.69. ESI-HRMS $[M+H]^+$ calcd for $C_{15}H_{16}NO_5$ 290.1023, found: 290.1028.

*4.2. Biological evaluation*

*4.2.1. Cell lines culture*

All cancer cell lines (MDA-MB-231, MDA-MB-468 and HepG2) were purchased from the Cell Bank of Shanghai Institute of Cell Biology, Chinese Academy of Sciences (Shanghai, China). The MDA-MB-231 and MDA-MB-468 cell lines were cultured in Dulbecco Modified Eagle Medium/ Nutrient Mixture F-12(DMEM/F-12, Biological Industries, Beit Haemek, Israel), supplemented with 10% (v/v) fetal bovine serum (FBS, Gibco), 50 mg/mL penicillin and 50 mg/ mL streptomycin (Biological Industries, Beit Haemek, Israel). While the HepG2 cell line was maintained in high glucose Dulbecco's Modified Eagle Medium (Biological Industries, Beit Haemek, Israel) replenished with 10% fetal bovine serum, and penicillin/streptomycin. All the cell lines were incubated at 37 □ in a humidified atmosphere containing 5% $CO_2$.

*4.2.2. In vitro cell growth inhibitory activity assays*

All of these cancer cells were seeded in 96-well culture plates at a density of 5000-7000 cells per well (100 μL/well) and incubated at 37 □ in a humidified atmosphere containing 5% $CO_2$ for 8h. In succession, different concentrations of test compounds were added in triplicate to the plates in 100 μL fresh mediums (the total volume was 200 μL, DMSO <0.1%) and incubated at 37 □ for 48 h. After removing the cell culture medium, 10% Cell Counting Kit-8 (CCK-8, APExBIO, Houston, USA) solution (100 μL) was administered in the 96-well plates and re-incubated for 4 h (MDA-MB-468, MDA-MB-231) and 1h (HepG2). Finally, the absorbance was measured at the wavelength of 450 nm by a microplate spectrophotometer (MK3, Thermo, Germany). Each treatment was performed in triplicate. The half inhibitory concentration $IC_{50}$ values were calculated by Prism 7.0 (GraphPad Software).

*4.2.3. Fluorescence polarization assay*

The STAT3 protein (His-tag 127-722 amino acid, DetaiBio, China) was diluted to a concentration of 1600 nM and the fluorescently labelled peptide probe (5-FAM-GpYLPQTV-NH2, ChinaPeptides, China) was deliquated to a concentration of 100 nM. Different concentrations of tested compound (10 μL) and prepared STAT3 protein (10 μL) were added to 70 μL assay buffer (Hepes 10 mM PH=7.5, EDTA 1 mM, NaCl 50 mM, 0.1% Nonidet P40) in 96-well, black round-bottom plates at 37 □ for 30 minutes. Then 10 μL of fluorescently labelled peptide probe was added and incubated at 37 □ for another 1 h. The polarization values were measured at an excitation wavelength of 485 nm and an emission wavelength of 530 nm, which was detected by Tecan Spark instrument. The half inhibitory concentration $IC_{50}$ values were by Prism 7.0 (GraphPad Software).

*4.2.4. Western blot analysis*

MDA-MB-231 cells were incubated with various concentrations of compound **A11** for 24 h and rinsed twice with PBS and then lysed with RIPA buffer (Beyotime Biotechnology) containing a protease inhibitor (PMSF) mixture at 1:100 dilution on

ice for 10 min. The lysates were cleared by centrifugation (4 □, 12,000 rmp,10 min), and BCA protein assay kit was applied to measure the protein concentration. Equal amount of proteins from the total cell lysates (40 μg per lane) was separated by sodium dodecyl sulfate (10 %) polyacrylamide gel electrophoresis (SDS-PAGE, BioRad Laboratories, Hercules, CA), and then electrically transferred to polyvinylidene difluoride (PVDF) membranes (BioRad Laboratories, Hercules, CA). The membranes were blocked with 5% non-fat powdered milk in TBST buffer for 2 h at room temperature, and blotted with primary antibodies specific for STAT3, p-STAT3(Y705), STAT1, p-STAT1(Y701), C-Myc, Cyclin D1 and GAPDH at 4 □ for overnight. After washing out three times (5 min each) with TBST, the corresponding HRP-conjugated secondary antibodies were incubated for 1h at room temperature. Enhanced chemiluminescence (ECL) and bioanalytical imaging system (Azure biosystems, Inc, C600) were applied for assay of target proteins.

*4.2.5. Cell immunofluorescent assay*

After MDA-MB-231 cells were cultured and incubated in confocal dishes at a density of $1\times10^4$ cells per dish overnight, compound **A11** was added and incubated for 24 h. Then, cells were fixed with 4 % paraformaldehyde and permeabilized with 0.5 % Triton X-100 for 15 min respectively. Subsequently, they were sealed with 5% BSA for 1 h and fostered with the specific primary antibody against STAT3 overnight at 4°C. Next, the Alexa-conjugated secondary antibody (Alexa Fluor 546 goat anti-rabbit IgG, Invitrogen, A-11035) was added and incubated at room temperature for 1 h. Cell nucleus were stained with Hoechst for 10 min. Finally, the cells images were tested and analyzed by a fluorescence microscope (Nikon Eclipse Ti2).

*4.2.6. Flow cytometry analysis of apoptotic cells*

MDA-MB-231 cells at a density of $2\times10^5$ per well were cultured in regular growth medium in 6-well plates for 24 h and disposed in duplicate with various concentrations of compound **A11** for 24 h. Then the cells were trypsinized, was rinsed twice with PBS (centrifugation at 2000 rpm, 5 min) and collected for the next step.

After resuspending the cells in 500 μL of binding buffer, 5 μL Annexin V-FITC and 5 μL propidium iodide were added and mixed gently. Finally, the mixture was incubated for 15 min at room temperature in dark and detected by a flow cytometer (Beckman coulter, Inc, A00-1-1102).

*4.2.7 cell cycle effect*

MDA-MB-231 cells were seeded in 6-well plates at density of $2\times10^5$ cells/well. After overnight adherence, they were incubated with various concentrations of **A11** for 24h. The treated cells were collected by centrifugation, washed with PBS and fixed in ice-cold 70% ethanol. Then incubated for 30 min at 37°C with PI containing RNase (MA0334, Dalian Meilun Biotdchnology Co, LTD). The samples were then analyzed by flow cytometry (Beckman coulter, Inc, A00-1-1102).

*4.2.8. In vivo studies*

All procedures were performed according to the National Institutes of Health Guidelines for the Care and Use of Laboratory Animals and were approved by the local animal ethics committees. Human breast tumor MDA-MB-231cells ($5\times10^6$) were injected into the subcutaneous tissue of five weeks old female BALB/c nude mice (16–18g). When the tumor volume reached around 50 $mm^3$, the mice were randomly classified into three groups (six mice per group) and intraperitoneally treated with compound **A11** at a dosage of 5 mg/kg or 10 mg/kg daily for 21 days. Simultaneity, the tumor volume was measured once every three days and numerated by the formula: length × $width^2/2$, and the body weight of mice was meted and registered. At terminal phase, all mice were sacrificed and the tumor was segregated, and weighed. The levels of p-STAT3 in tumor tissues were analyzed by the immunofluorescent assay.

*4.2.9. Tissue immunofluorescent assay*

The pre-treated and fixed tumor sections were incubated with antibody against p-STAT3 at 4 □ overnight. After scouring with PBST three times, the

Alexa-conjugated secondary antibody (Cy3-AffiniPure Goat Anti-Rabbit IgG(H+L), Jackson, 111-165-003) was added and reared at 37 □ for 40 minutes. Cell nucleus was dyed with DAPI (4', 6-Diamidino-2-Phenylindole) for 10 min. Finally, the cells images were detected and resolved by a fluorescence microscope (Nikon Eclipse Ti2).

*4.3. Molecular docking*

Molecular docking study was executed applying Schrodinger software package. Firstly, the X-ray crystal structure of STAT3 was retrieved from Protein Data Bank (PDB code: 1BG1) and prepared with the Protein Preparation Wizard model including the removement of one monomer, the addition of missing hydrogen atoms, the assignment of bond order, assessment of the correct protonation states, and a restrained minimization using the OPLS-2005 force field. Then, the receptor grid was generated at the centroid of selected residues (LYS591, ARG595) and the grid box size was set to 20 Å. After preparing the ligands, molecular docking was carried out using the standard precision (SP) with the default settings. Finally, the pictures were generated using pymol software.

*4.4. X-ray crystal structure determination of compound **A24***

The D8 venture diffractometer view of compound **A24** is shown in Fig. 4. The crystal data and structure refinement were emerged in supporting information. The compound was crystallized in the monoclinic space group P2(1)/c with 4 molecules in the unit cell and the structure was solved by direct method with the SHELXTL program package. All the crystallographic parameters (excluding structure factors) of this structure have been deposited in the Cambridge Crystallographic Data Center as supplementary publication number CCDC 1973547. Copies of the data can be obtained, free of charge, on application to CCDC, 12 Union Road, Cambridge CB2 1EZ, UK [fax: +44 (0) 223 336033 or e-mail: deposit@ccdc.cam.ac.uk.

**Declaration of competing interest**

The authors declare that they have no known competing financial interests or personal relationships that could have appeared to influence the work reported in this paper.

**Acknowledgement**

Financial support was generously provided by the National Natural Science Foundation of China (Nos. 81903423 and 21871184), the China Postdoctoral Science Foundation (2018M642064), the Shanghai Sailing Program (19YF1449300), the Shanghai Municipal Education Commission (2019-01-07-00-10-E00072), and the Science and Technology Commission of Shanghai Municipality (18401933500).

**Appendix A. Supplementary data**

Supplementary data related to this article can be found at

**Reference**

[1] [1] J.E.Jr. Darnell, Transcription factors as targets for cancer therapy, Nat. Rev. Cancer 2 (2002) 740–749.

[2] G. Miklossy, T.S. Hilliard, J. Turkson, Therapeutic modulators of STAT signaling for human diseases, Nat. Rev. Drug Discov. 12 (2013) 611-629.

[3] S. Fletcher, J.A. Drewry, V.M. Shahani, B.D. Page, Molecular disruption of oncogenic signal transducer and activator of transcription 3 (STAT3) protein, Biochem. Cell. Biol. 87 (2009) 825-833.

[4] B.E. Barton, J.G. Karras, T.F. Murphy, A. Barton, H.F. Huang, Signal transducer and activator of transcription 3 (STAT3) activation in prostate cancer: direct STAT3 inhibition induces apoptosis in prostate cancer lines, Mol. Cancer Ther. 3 (2004) 11-20.

[5] H. Yu, R. Jove, The STATs of cancer: new molecular targets come of age, Nat. Rev. Cancer 4 (2004) 97-105.

[6] H. Yu, H. Lee, A. Hermann, R. Buenttner, R. Jove, Revisiting STAT3 signalling in cancer: new and unexpected biological functions, Nat. Rev. Cancer. 14 (2014) 737-746.

[7] J. Turkson, D. Ryan, J.S. Kim, Y. Zhang, Z. Chen, E. Haura, A. Laundano, S. Sebti, A.D. Hamilton, R. Jove, Phosphotyrosyl peptides block Stat3-mediated DNA binding activity, gene regulation, and cell transformation, J. Biol. Chem. 276 (2001) 45443-45455.

[8] J.M. McDaniel, K.E. Varley, J. Gertz, D.S. Savic, B.S. Roberts, S.K. Bailey, L.A. Shevde, R.C. Ramaker, B.N. Lasseigne, M.K. Kirby, K.M. Newberry, E.C. Partridge, A.L. Jones, B. Boone, S.E. Levy, P.G. Oliver, K.C. Sexton, W.E. Grizzle, A. Forero, D.J. Buchsbaum, S.J. Cooper, R.M. Myers, Genomic regulation of invasion by STAT3 in triple negative breast cancer, Oncotarget 8 (2017) 8226-8238.

[9] H.L. Koskela, S. Eldfors, P. Ellonen, A.J. van Adrichem, H. Kuusanmaki, E.I. Andersson, S. Lagstrom, M.J. Clemente, T. Olson, S.E. Jalkanen, M.M. Majumder, H. Almusa, H. Edgren, M. Lepisto, P. Mattila, K. Guinta, P. Koistinen, T. Kuittinen, K. Penttinen, A. Parsons, J. Knowles, J. Saarela, K. Wennerberg, O. Kallioniemi, K. Porkka, T.P. Loughran, C.A. Heckman, J.P. Maciejewski, S. Mustjoki, Somatic STAT3 mutations in large granular lymphocytic leukemia, N. Engl. J. Med. 366 (2012) 1905-1913

[10] H. Yu, M. Kortylewski, D. Pardoll, Crosstalk between cancer and immune cells: role of STAT3 in the tumour microenvironment, Nat. Rev. Immunol. 7 (2007) 41-51.

[11] A.V. Villarino, Y. Kanno, J.R. Ferdinand, J.J. O'Shea, Mechanisms of Jak/STAT signaling in immunity and disease, J. Immunol. 194 (2015) 21-27.

[12] D.E. Johnson, R.A. O'Keefe, J.R. Grandis, Targeting the IL-6/JAK/STAT3 signalling axis in cancer, Nat. Rev. Clin. Oncol. 15 (2018) 234-248.

[13] J.E. Darnell Jr., Transcription factors as targets for cancer therapy, Nat. Rev. Cancer 2 (2002) 740-749

[14] Q. Huang, Y. Zhong, H. Dong, Q. Zheng, S. Shi, K. Zhu, X. Qu, W. Hu, X. Zhang, Y. Wang, Revisiting signal transducer and activator of transcription 3 (STAT3) as an anticancer target and its inhibitor discovery: Where are we and where should we go? Eur. J. Med. Chem. 187 (2020) DOI: 10.1016/j.ejmech.2019.111922.

[15] H. Song, R. Wang, S. Wang, J. Lin, A low-molecular weight compound discovered through virtual database screening inhibits Stat3 function in breast cancer cells, Proc. Natl. Acad. Sci. U. S. A. 102 (2005) 4700-4705.

[16] L. Lin, B. Hutzen, P.K. Li, S. Ball, M. Zuo, S. DeAngelis, E. Foust, M. Sobo, L. Friedman, D. Bhasin, L. Cen, C. Li, J. Lin, A novel small molecule, LLL12, inhibits STAT3 phosphorylation and activities and exhibits potent growth-suppressive activity in human cancer cells, Neoplasia 12 (2010) 39-50.

[17] W. Yu, H. Xiao, J. Lin, C. Li, Discovery of novel STAT3 small molecule inhibitors via in silico site-directed fragment-based drug design, J. Med. Chem. 56 (2013) 4402-4412.

[18] J. Schust, B. Sperl, A. Hollis, T.U. Mayer, T. Berg, Stattic: a small-molecule inhibitor of STAT3 activation and dimerization, Chem. Biol. 13 (2006) 1235-1242.

[19] X. Ren, L. Duan, Q. He, Z. Zhang, Y. Zhou, D. Wu, J. Pan, D. Pei, K. Ding, Identification of niclosamide as a new small-molecule inhibitor of the STAT3 signaling pathway, ACS Med. Chem. Lett. 1 (2010) 454-459.

[20] K. Siddiquee, S. Zhang, W.C. Guida, M.A. Blaskovich, B. Greedy, H.R. Lawrence, M.L. Yip, R. Jove, M.M. McLaughlin, N.J. Lawrence, M.S. Sebti, J. Turkson, Selective chemical probe inhibitor of Stat3, identified through structure-based virtual screening, induces antitumor activity, Proc. Natl. Acad. Sci. U. S. A. 104 (2007) 7391-7396.

[21] X. Zhang, P. Yue, S. Fletcher, W. Zhao, P.T. Gunning, J. Turkson, A novel small-molecule disrupts Stat3 SH2 domain-phosphotyrosine interactions and Stat3-dependent tumor processes, Biochem. Pharmacol. 79 (2010) 1398-1409.

[22] W. Yu, C. Li, W. Zhang, Y. Xia, S. Li, J.Y. Lin, K. Yu, M. Liu, L. Yang, J. Luo, Y. Chen, H. Sun, L. Kong, Discovery of an orally selective inhibitor of signal transducer and activator of transcription 3 using advanced multiple ligand simultaneous docking, J. Med. Chem. 60 (2017) 2718-2731.

[23] Y. Li, H.A. Rogoff, S. Keates, Y. Gao, S. Murikipudi, K. Mikule, D. Leggett, W. Li, A.B. Pardee, C.J. Li, Suppression of cancer relapse and metastasis by inhibiting cancer stemness, Proc. Natl. Acad. Sci. U. S. A. 112 (2015) 1839-1844.

[24] J. Guo, W. Yu, G. Cai, W. Zhang, S. Li, J. Zhu, D. Song, L. Kong, Discovery of new benzensulfonamide derivatives as tripedal STAT3 inhibitors, Eur. J. Med. Chem. 151 (2018) 752-764.

[25] W. Zhang, T. Ma, S. Li, Y. Yang, J. Guo, W. Yu, L. Kong, Antagonizing STAT3 activation with benzo[b]thiophene 1, 1-dioxide based small molecules, Eur. J. Med. Chem. 125 (2017) 538-550.

[26] G. Cai, W. Yu, D. Song, W. Zhang, J. Guo, J. Zhu, Y. Ren, L. Kong, Discovery of fluorescent coumarin-benzo[b]thiophene 1, 1-dioxide conjugates as mitochondria-targeting antitumor STAT3 inhibitors, Eur. J. Med. Chem. 174 (2019) 236-251.

[27] W. Zhang, W. Yu, G. Cai, J. Zhu, C. Zhang, S. Li, J. Guo, G. Yin, C. Chen, L. Kong, A new synthetic derivative of cryptotanshinone KYZ3 as STAT3 inhibitor for triple-negative breast cancer therapy, Cell Death Dis. 9 (2018) 1098.

[28] M. Zhang, W. Zhu, Y. Li, Discovery of novel inhibitors of signal transducer and activator of transcription 3 (STAT3) signaling pathway by virtual screening, Eur. J. Med. Chem. 62 (2013) 301-310.

[29] D. Gao, Q. Xiao, M. Zhang, Y. Li, Design, synthesis and biological evaluation of benzyloxyphenyl-methylaminophenol derivatives as STAT3 signaling pathway inhibitors, Bioorg. Med. Chem. 24 (2016) 2549-2558.

[30] M. Lai, H. Lee, H. Chuang, L. Chang, A. Tsai, M. Chen, H. Huang, Y. Wu, C. Teng, S. Pan, Y. Liu, S. Mehndiratta, J. Liou, N-Sulfonyl-aminobiaryls as Antitubulin Agents and Inhibitors of Signal Transducers and Activators of Transcription 3 (STAT3) Signaling, J. Med. Chem. 58 (2015) 6549-6558.

[31] X. Wang, Q. He, K. Wu, T. Guo, X. Du, H. Zhang, L. Fang, N. Zheng, Q. Zhang, F. Ye, Design, synthesis and activity of novel 2,6-disubstituted purine derivatives, potential small molecule inhibitors of signal transducer and activator of transcription 3, Eur. J. Med. Chem. 179 (2019) 218-232.

[32] L. Bai, H. Zhou, R. Xu, Y. Zhao, K. Chinnaswamy, D. McEachern, J. Chen, C.Y. Yang, Z. Liu, M. Wang, L. Liu, H. Jiang, B. Wen, P. Kumar, J.L. Meagher, D. Sun, J.A. Stuckey, S. Wang, A potent and selective small-molecule degrader of STAT3 achieves complete tumor regression in vivo, Cancer Cell 36 (2019) 498-511.

[33] H. Zhou, L. Bai, R. Xu, Y. Zhao, J. Chen, D. McEachern, K. Chinnaswamy, B. Wen, L. Dai, P. Kumar, C. Yang, Z. Liu, M. Wang, L. Liu, J.L. Meagher, H. Yi, D. Sun, J.A. Stuckey, S. Wang, Structure-based discovery of SD-36 as a potent, selective, and efficacious PROTAC degrader of STAT3 protein, J. Med. Chem. 62 (2019) 11280-11300.

[34] J.D. Beebe, J.Y. Liu, J.T. Zhang, Two decades of research in discovery of anticancer drugs targeting STAT3, how close are we? Pharmacol Ther. 191 (2018) 74-91.

[35] S.L. Furtek, D.S. Backos, C.J. Matheson, P. Reigan, Strategies and approaches of targeting STAT3 for cancer treatment, ACS Chem. Biol. 11 (2016) 308-318.

[36] B. Debnath, S. Xu, N. Neamati, Small molecule inhibitors of signal transducer and activator of transcription 3 (Stat3) protein, J. Med. Chem. 55 (2012) 6645-6668.

[37] https://www.cancer.gov/about-cancer/treatment/clinical-trials/intervention/napabucasin

[38] C. Li, C. Chen, Q. An, T. Yang, Z. Sang, Y. Yang, Y. Ju, A. Tong, Y. Luo, A novel series of napabucasin derivatives as orally active inhibitors of signal transducer and activator of transcription 3 (STAT3), Eur. J. Med. Chem. 162 (2019) 543-554.

[39] Q. Zhou, C. Peng, F. Du, L. Zhou, Y. Shi, Y. Du, D. Liu, W. Sun, M. Zhang, G. Chen, Design, synthesis and activity of BBI608 derivatives targeting on stem cells, Eur. J. Med. Chem. 151 (2018) 39-50.

[40] A. Reichstein, S. Vortherms, S. Bannwitz, J. Tentrop, H. Prinz, K. Muller, Synthesis and structure-activity relationships of lapacho analogues. 1. Suppression of human keratinocyte hyperproliferation by 2-substituted naphtho[2,3-b]furan-4,9-diones, activation by enzymatic one- and two-electron reduction, and intracellular generation of superoxide, J. Med. Chem. 55 (2012) 7273-7284.

[41] S. Bannwitz, D. Krane, S. Vortherms, T. Kalin, C. Lindenschmidt, N. Zahedi Golpayegani, J. Tentrop, H. Prinz, K. Muller, Synthesis and structure-activity relationships of lapacho analogues. 2. Modification of the basic naphtho[2,3-b]furan-4,9-dione, redox activation, and suppression of human keratinocyte hyperproliferation by 8-hydroxynaphtho[2,3-b]thiophene-4,9-diones, J. Med. Chem. 57 (2014) 6226-6239.

[42] T. Sone, W. Hirose, N. Shimada, C.J. Li, W. Li, D. Leggett, 3-substituted Carbonyl-naphtho[2,3-b]furane Derivative or Pharmaceutically Acceptable Salt Thereof, 2015. WO 2015/12030.

[43] X. Cai, X. B. Zhong, Process for preparation of furo[2,3-g]quinoline-4,9-dione compound and medical application, Faming Zhuanli Shenqing (2017), CN107501279A20171222. Language: Chinese, Database: Caplus.

[44] K. Bolibrukh, O. Khoumeri, S. V. Polovkovych, V. Novikov, T. Terme, P. Vanelle, Novel synthesis of 5-Substituted 5H-benzo[b]carbazole-6,11-diones via double Buchwald–Hartwig reaction, Synlett 25 (2014) 2765-2768.

[45] A. Borah, A. Sharma, H. Hazarika, K. Sharma, P. Gogoi, Synthesis of 1-azaanthraquinone: sequential C–N bond formation/lewis acid catalyzed intramolecular cyclization strategy, J. Org. Chem. 82 (2017) 8309-8316.

[46] CCDC 1973547 (A24) contains the supplementary crystallographic data for this paper. These data can be obtained free of charge from The Cambridge Crystallographic Data Centre via www.ccdc.cam.ac.uk/data_request/cif.

[47] J. Schust, T. Berg, A high-throughput fluorescence polarization assay for signal transducer and activator of transcription 3, Anal Biochem. 330 (2004) 114-118.

## Highlights:

1. Novel scaffold and high potency of **A11** as selective STAT3 inhibitor was discovered by applying a structure-based design strategy.
2. Compound **A11** could inhibit the activation of STAT3 (Y705) and thus reduced the expression of STAT3 downstream gene CyclinD1 and C-Myc.
3. Compound **A11** could suppress the MDA-MB-231 xenograft tumor growth in mice at the dosage of 10 mg/kg (i.p.) without obvious body weight loss.
4. Molecular docking study elucidated the binding mode of **A11** in STAT3 SH2 domain.

## Declaration of competing interest

The authors declare that they have no known competing financial interests or personal relationships that could have appeared to influence the work reported in this paper.